# Millimeter-Scale Diffractive Optical Elements Fabricated by Two-Photon Polymerization for Beam Shaping in Materials Processing

Felix Behlau\*†, Jan Marx†, Leonie Zimmermann, Tobias Thüsing, Elia Albini, Cemal Esen, and Andreas Ostendorf

Applied Laser Technologies, Ruhr University Bochum,
Universitätsstr. 150, 44801 Bochum, Germany
\*Corresponding author's e-mail: <a href="mailto:felix.behlau@ruhr-uni-bochum.de">felix.behlau@ruhr-uni-bochum.de</a>
†These authors contributed equally to this work.

Beam shaping is a crucial aspect in the field of laser materials processing. Among the optical elements available for this purpose, Diffractive Optical Elements (DOEs) stand out due to their robustness and versatility. However, a flexible fabrication method is desirable to facilitate rapid testing of different beam shapes using various DOEs. Two-Photon Polymerization (2PP) is a promising fabrication technology for this purpose, as it allows the creation of arbitrarily shaped three-dimensional structures with a resolution down to 100 nm and excellent surface quality. In this work, a DOE was fabricated using 2PP, which modulates the light into a set of two ring beams. The phase input was calculated as a computer-generated hologram using the prism and lens algorithm, where the term for the axial focus shift was substituted by an axicon hologram. The DOE has a diameter of 3.5 mm and a maximum height of 6.4 µm. To fabricate this DOE, the phase input image was converted into a corresponding three-dimensional STL file depending on the gray level of each hologram pixel. After fabrication, beam shaping properties of the DOE were analyzed using a beam profiler to visualize the resulting two ring beams. Damage threshold experiments validated the robustness of the DOE for material processing.

DOI: 10.2961/jlmn.2025.03.2008

**Keywords:** two-photon polymerization, diffractive optical element, beam shaping, axicon, Bessel beam, materials processing

# 1. Introduction

The ability to shape laser beams is of critical importance for laser-based materials processing technologies. The capacity to modify the spatial intensity profile of a laser beam facilitates the customization of the beam to suit particular processing applications, thereby enhancing beam quality [1, 2], efficiency [3, 4], and flexibility [5]. A variety of optical components have been developed to address this need, with Diffractive Optical Elements (DOEs) emerging as one of the most robust and versatile solutions [6].

DOEs have the capability to encode complex phase functions in a single element, thereby enabling advanced beam manipulation, including splitting, shaping, and focusing. The flexibility of these functions makes them well-suited for the generation of multiple beams, non-Gaussian profiles, and propagation-invariant beams like Bessel beams. However, conventional fabrication methods, including photolithography [7], electron beam lithography [8], nanoimprint lithography [9], ion beam milling [10], and reactive ion etching [11], are frequently constrained by factors such as high cost, inflexibility, or slow prototyping.

To overcome these limitations, additive microfabrication techniques have gained attention as an alternative approach for the production of complex freeform optics. Among them, Two-Photon Polymerization (2PP) stands out due to its capability to fabricate arbitrary three-dimensional structures with sub-micrometer resolution and high surface quality [12]. This technique relies on the nonlinear absorption of femtosecond laser pulses to induce localized polymerization

within a photoresist, allowing for the direct writing of intricate micro-optical components [13]. Since only a spatially limited part of the focal volume exhibits a sufficient photon density to induce a polymerization reaction inside the material, feature sizes below the diffraction limit can be achieved [14]. Thus, this degree of precision and design freedom offered by 2PP makes it an ideal candidate for the rapid prototyping of custom DOEs tailored to specific beam shaping applications, as it was already shown by multiple research groups [15-18].

In this study, we explore the use of 2PP to fabricate DOEs designed to generate multiple Bessel beams. Bessel beams are of particular interest due to their non-diffracting properties, which make them advantageous in applications such as precision drilling [19, 20], and volumetric modification of transparent materials [21]. However, many Bessel beam-based applications suffer from low process speeds, as the combination of axicons and scanner optics is difficult to implement. Therefore, there is significant interest in multibeam elements, which can be used for parallel processing [20]. Furthermore, axicons are often integrated into compact systems such as endoscopic devices [22, 23], where the combination of axicons with additional optical beam shaping elements is of high interest to maintain the compactness of the system. The phase profiles required to produce these beams were computed using the prism and lens algorithm described by Liesener et al. [24], modified by replacing the axial focusshift term with a holographic axicon component [25] to achieve the desired Bessel beam structure. However, the

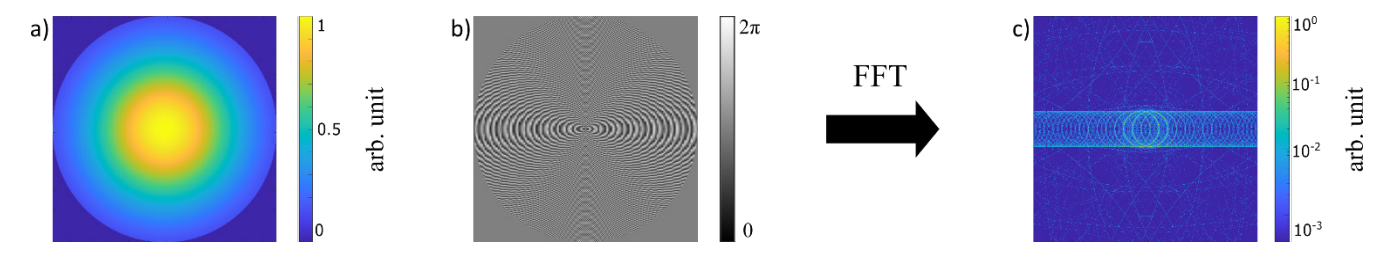


**Fig. 1** (a) Amplitude distribution and (b) phase image in the hologram plane. (c) Amplitude of the Fourier transformation of the input beam shows the intensity in the far field behind the DOE.

characterization of Bessel beams in the near field behind an axicon proves to be challenging due to the very small spot dimensions, which are on the order of the pixels of beam profilers. For this reason, in the context of this work, the ring beams in the far field of the DOE were characterized, whose uniformity also provides insights into the beam shaping capabilities of the DOE. The ability of 2PP-printed Fresnel axicons to form a Bessel beam before the ring beam has already been confirmed in a previous work [18].

In this paper we demonstrate the fabrication of such a DOE with a diameter of 3.5 mm and a maximum structure height of 6.4 µm. By fabricating DOEs with these dimensions, a research gap is closed by increasing the lateral extent and thus the maximum usable laser power compared to previous printed micro-optics while simultaneously preserving the high resolution of the 2PP process. The manufacturing of the DOE required approximately 68.5 hours and involved the conversion of the calculated phase input into a three-dimensional STL model. This STL-file was split to match the full field of view of the objective lens used in the printing system.

Following fabrication, the beam shaping performance of the DOE was evaluated using a beam profiler. The DOE's effectiveness in generating multiple ring beams was assessed, and its suitability for laser micro material processing was further validated through damage threshold measurements.

## 2. Calculation of DOE

A self-written software [26] based on Matlab (Matlab 2023a, Mathworks Inc.) was used to generate the STL-file for the printing process. In the first step, a computer-generated phase hologram (CGH) was calculated describing the shape of the DOE. A Gaussian beam profile with a diameter of 3.5 mm (1/e²) was used as amplitude distribution in the hologram plane. An aperture with a diameter of 3.5 mm was used to cut off peripheral rays. The described input beam is shown in Figure 1 (a). A matrix consisting of 5833 x 5833 values was describing the height of the DOE across its cross section. Considering the diameter of the DOE of 3.5 mm, this results in a pixel size of 600 nm.

As an example of the DOE fabricated in this work, a CGH was selected, which transforms a Gaussian input beam into a pair of adjacent ring-shaped beams in the far field of the DOE. In the near field behind the DOE, two Bessel beams are formed. For the calculation of the CGH, the prism and lens algorithm by Liesener et al. [24] was employed, which allows an input beam to be split into multiple beams, with individual focal points being shifted laterally by the prism term and axially by the lens term. In contrast to the

conventional algorithm, for the CGH calculated here, the lens term was replaced by an axicon term, which facilitates the transformation of the Gaussian beam into a Bessel or ring beam, respectively [25]. The axicon angle was set to 6°. The characteristics of an axicon CGH are described in prior publication [18].

Outside the desired DOE diameter of 3.5 mm, all values of the hologram matrix were set to a constant value to get a circular DOE instead of a square-shaped one. The resulting CGH is shown in Figure 1 (b).

Subsequently, the CGH was utilized to generate an STL file from the grayscale matrix, which can be employed in the 2PP fabrication process. For the calculation of the STL file, each pixel was assigned a height according to its grayscale value, resulting in points with three coordinates. The maximum height (white pixels) was 6.4  $\mu m$ , while the minimum height (black pixels) was 2  $\mu m$ . This results in a structure height of  $h=4.4~\mu m$ , which equals a modulation depth according to equation 1.

Modulation Depth := 
$$\frac{(n-n_0)\cdot h}{\lambda} \approx 3$$
, (1)

where n = 1.55 is the refraction index of the cured 2PP photoresist [27],  $n_0 \approx 1$  is the refraction index of the surrounding medium and  $\lambda = 800$  nm is the laser wavelength of the input beam. This results in a phase shift of the DOE of  $6\pi$ . The chosen modulation depth represents a compromise between high diffraction efficiency (better with greater modulation depth) and shorter printing time (better with lower modulation depth).

In a last step, the points of the pixels were connected to a surface and further points at the side and bottom of the DOE were added to make the STL define a closed volume.

The resulting amplitude distribution in the farfield  $A_{farfield}$  of the DOE is shown in Figure 1 (c). It was calculated by a Fast Fourier Transformation of the input amplitude  $A_i$  and input phase  $\phi_i$  according to equation 2:

$$A_{farfied} = |FFT(A_i e^{i\phi_i})|. \tag{2}$$

The two ring beams can be seen clearly in the farfield amplitude distribution. Besides that, there are more rings with lower intensity indicating the higher order maxima of the CGH.

## 3. 2PP Fabrication of DOE

The 2PP setup used for the DOE fabrication is described in detail in [28] and consists of an ultrashort pulse Ti:Sa laser (Tsunami, Spectra-Physics Inc.), three linear axes (Wafer Max Z and ANT 130-XY, Aerotech Inc.), and a Galvo scanner (hurrySCAN II 14, SCANLAB GmbH). The utilized laser source operates at a repetition rate of 82 MHz, with a pulse length of 100 fs and a central wavelength of 780 nm.

A microscope objective (20x NA=0.8 Plan-Apochromat, Carl Zeiss Microscopy Germany GmbH) with a large field of view (FOV) of 500  $\mu m$  x 500  $\mu m$  was utilized to facilitate the fabrication of millimeter-scale optical elements within a reasonable timeframe. Accordingly, the STL file derived from the DOE is divided into 49 squares, with each square measuring 500  $\mu m$  x 500  $\mu m$ . The arrangement of these squares in a 7x7 grid of stitching tiles corresponds to the DOE diameter of 3.5 mm.

The fabrication of each square is executed in a sequential manner, employing a layer-by-layer approach. The fabrication of each layer is conducted using the Galvo scanner. Subsequent to the fabrication of each layer, the sample is positioned for the subsequent layer by the axis system. After the fabrication of one square, the axis system is employed to position the sample for the subsequent square.

Due to the inherent axis tolerances and limitations in the fabrication of the sample holder and glass substrate, the samples can only be positioned in a not perfectly perpendicular orientation relative to the microscope objective. Thus, the initial point of intersection between the photoresist and glass, which serves as the starting point for the print, exhibits variability across the printing area. As small deviations in perpendicularity over an area of 3.5 mm x 3.5 mm showed significant height errors of several micrometers, which is equivalent to the total structure height, a tilt correction was implemented. The starting point was determined at three distinct locations on the glass substrate, and a plane intersecting those three points was subsequently calculated. During the fabrication process, the initial position of each fabricated square was adjusted in relation to the first square, with the adjustment being proportional to the plane. Moreover, the minimum pixel height of the DOE was established at 2 µm, thereby ensuring the presence of a 2 µm thick base below the DOE structure, which serves as an error tolerance.

The DOE was fabricated with the photoresist FemtoBond 4B (Laserzentrum Hannover e.V., Germany) and its fabrication required a total of 68.5 hours. All relevant process parameters are listed in Table 1.

 Table 1
 2PP process parameters

Parameter	Value
Average laser power	25 mW
Laser scan speed	10  mm/s
Layer thickness	0.1 µm
Hatch distance	0.3 µm
Material	FemtoBond

Figure 2 shows a light microscope image of the DOE at a magnification of 2.5x. The calculated phase map is clearly identifiable in the fabricated DOE. A small hole is visible in

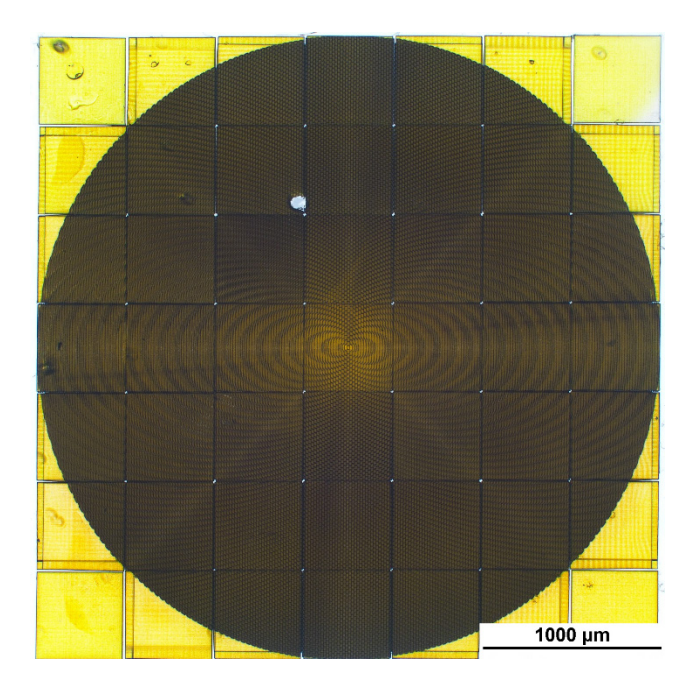


**Fig. 2** Light microscope image of the DOE at 2.5x magnification.

the upper left side of the DOE. However, as shown in [18], the effect of such holes is negligible for beam shaping. The hole could potentially be caused by a dust particle adhered to the glass substrate prior to the application of the photoresist. Furthermore, small holes are visible at the corners of the areas. These holes may have been caused by an error in the calculation during the slicing process.

The central section of the DOE is illustrated in Figure 3 through an SEM image at a 45° angle. The calculated height differences of the individual pixels in the calculated DOE phase map are clearly visible. Nonetheless, a discernible staircase effect and a substantial surface roughness are evident. The observed effects can be attributed to the utilization of a microscope objective with an NA value of 0.8, which possesses a considerably lower resolution in comparison to objectives with higher NA values. In contrast, such objectives offer a substantially larger FOV, thereby facilitating the

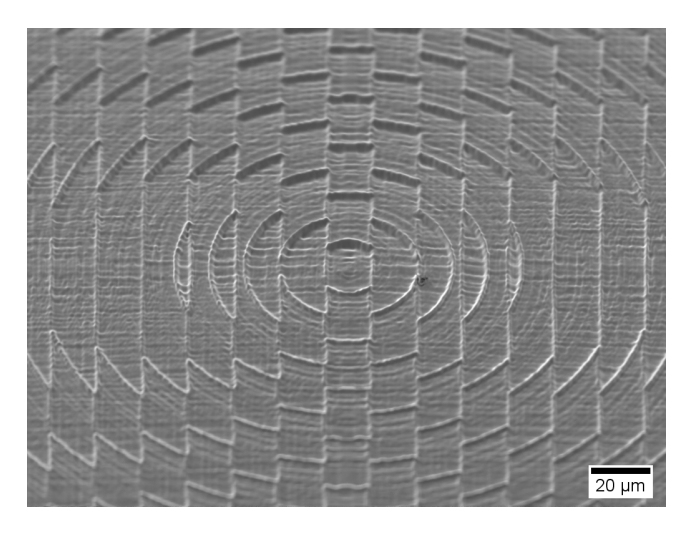


**Fig. 3** Scanning electron microscope image of the DOE center at 1000x magnification at a 45° angle.

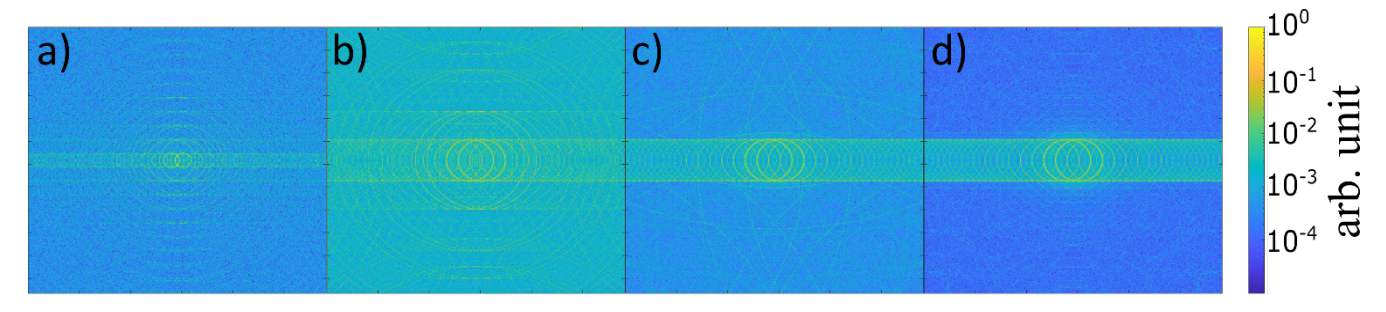


**Fig. 4** Simulated far field amplitude with different numbers of layer and different layer heights, respectively. a) 2 layers, 4.4 μm layer height, b) 10 layers, 1.5 μm layer height, c) 45 layers, 100 nm layer height, d) 255 layers, 17 nm layer height.

efficient fabrication of large areas within a reasonable timeframe. However, a simulation is intended to show the impact of the staircase effect on the diffraction pattern. The simulation from Figure 1 was adjusted with respect to a variation in the discretization of the grayscale in the phase image, which corresponds to an adjustment in the number of layers and thus the layer height. The calculated far field intensity distributions for different number of layers and thus different layer heights are presented in Figure 4. As seen in Figures 4 (a) and 4 (b), increasing the layer height causes additional diffraction orders of the concentric grating of the axicon phase image to become more pronounced. These are characterized by differing diameters of the circles. This is particularly noticeable in Figure 4 (a), where a binary phase image was simulated, as the smallest circles representing the minus first diffraction order exhibit a similar intensity to the actual ring beams. In Figure 4 (c), which corresponds to the DOE implemented in the experiment with 45 layers, these higher diffraction orders are less dominant. A further reduction of the staircase effect by decreasing the layer height to 17 nm (255 layers, see Figure 4 (d)) results in a further reduction of artifacts in the intensity distribution, leading to a less noisy beam profile. Concluding the findings from this simulation, the choice of layer height is a compromise between diffraction efficiency in the first order and manufacturing time.

#### 4. Beam profile Analysis

The characterization of the beam shaping ability of the fabricated DOE was performed using a regenerative Ti:Sa amplifier laser system (Spitfire, Spectra Physics Inc.) with a central wavelength of 800 nm, a bandwidth of 60 nm, a repetition rate of 5 kHz, and a pulse width of 110 fs, which is a common source for micro drilling processes. The 8.3 mm raw beam (at 1/e², M²=1.1) was demagnified by a factor of 3 by a telescope. An aperture was placed between the laser and the telescope and was partially closed. This ensured that no rays transmitted the glass substrate outside the DOE, except for some diffracted rays.

The theoretical spatial intensity distribution behind an axicon can be calculated with equation 3 [29, 30]

$$I(r,z) = \frac{4\pi^2}{\lambda} \cdot tan^2(\alpha) \cdot (n-1)^2 \cdot z \cdot I_0 \cdot \exp\left(-2\left((n-1) \cdot z \cdot \frac{\tan(\alpha)}{D_0}\right)^2\right) \cdot J_0^2\left(\frac{2\pi}{\lambda} \cdot (n-1) \cdot r \cdot \tan(\alpha)\right),$$
(3)

where  $I_{\theta}$  is the on-axis intensity and  $J_{\theta}$  is the zero order Bessel function.

With the parameters given in prior sections, the calculated focal diameter of the described axicon is approximately 8 µm. According to Equation 3, the highest intensity is achieved at a distance of 12 mm from the DOE.

A beam camera (LaserCam-HR II-1/2", Coherent Corp.) was used to capture the beam profile. Since the focal diameter is on the same order of magnitude as the pixel size of the camera, and the camera cannot be positioned at the focal distance from the DOE due to its geometry, the intensity distribution of the ring beams in the far field is examined instead of the Bessel beam profile. The sensor was placed at a distance of 51 mm behind the DOE. Figure 5 shows the captured beam profile, which was composed of multiple individual images because the size of the beam profile exceeds the sensor size of the beam profiler. The software AutoStitch [31] was used for composing of the images.

The intersecting ring beams with diameters in the range of 10 mm are clearly identifiable in the beam profile. Additionally, the shape of the DOE is discernible within the intersection area of both rings. This could be attributed to the presence of undiffracted beams. Furthermore, some of the spots can be attributed to the diffraction grating given by the stitching gaps or phase jumps between adjacent stitching tiles caused by a slight tilt of the stitching tiles. In comparison to previous work [18], where the effect of the stitching

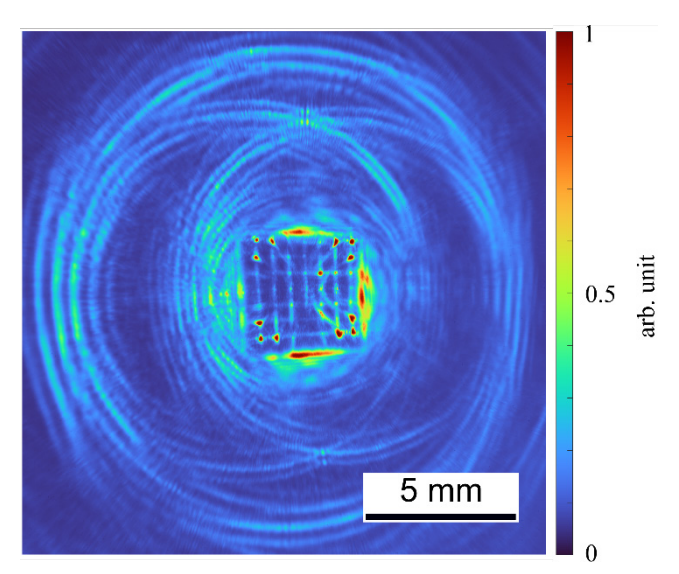


**Fig. 5.** Beam camera image measured 51 mm behind the DOE, which was illuminated by a Gaussian beam.

grid was thoroughly investigated through simulations, this effect is less pronounced here and largely overshadowed by other artifacts, as the stitching gaps were kept as small as possible. In particular, the corners of the individual areas demonstrate higher intensity, which may be attributed to the presence of small holes, where the beam is diffracted, as evidenced in Figure 2. Moreover, given that this beam profile does not employ a logarithmic scale, in contrast to the calculated amplitude depicted in Figure 1(c), it is not possible to detect higher order rings. Instead, one larger ring surrounding both rings is visible. The origin of this artefact might be a not perfect matched modulation depth of  $6\pi$ . Furthermore, the two ring beams consist of multiple rings spaced approx. 600 µm apart from each other instead of the one calculated. This phenomenon is a typical result of the generation of ring beams through the process of diffraction [18, 32].

## 5. Damage Test

The Ti:Sa laser, for which the DOE was designed, did not possess sufficient power to reach the damage threshold of the DOE. By applying 2 W average laser power (corresponds to 400 µJ pulse energy) at 800 nm, no damage was detected on the DOE. Consequently, an ultrashort pulse laser with a higher power (Carbide CB3-40W, Light Conversion, UAB) was utilized, featuring a pulse width of 191 fs, a repetition rate of 100 kHz, and a central wavelength of 1030 nm. The repetition rate was selected to achieve the highest possible pulse energy. The employment of a lens enabled the matching of the raw beam diameter to the DOE diameter of 3.5 mm. Subsequently, the power was increased in 5 % steps of the lasers maximum output power until the DOE was destroyed. Each power step was maintained for a duration of 30 seconds.

The DOE was able to withstand an average power of 22.8 W, which equates to a pulse energy of 228  $\mu$ J at a repetition frequency of 100 kHz. With regard to the irradiated area of the DOE, which has a diameter of 3.5 mm, a resulting peak power intensity of 24.8 GW/cm² could be calculated. The high damage threshold is potentially attributable to the thin thickness of 6.4  $\mu$ m of the DOE, which results in a reduction of laser absorption by the material.

The determined damage threshold of the DOE is comparable to the damage threshold study by Butkute et al. [33], in which a photoresist (SZ2080) of similar composition was used and a maximum laser fluence of  $17 \pm 9$  mJ/cm² was achieved when focusing a 1030 nm, 100 kHz, and 300 fs laser on bulk material with a height of 30  $\mu$ m. The maximum laser fluence of the DOE is 4.74 mJ/cm², indicating a slight discrepancy, yet the value remains within the same range.

# 6. Conclusion and outlook

The findings of this study demonstrate that 2PP-generated DOEs have the potential to be utilized in high-power applications. In order to achieve this objective, a number of significant factors were taken into consideration. Initially, an algorithm was developed that has the capacity to calculate custom DOEs and transform the phase map into 2PP printable STL files.

Secondly, by using a stitching algorithm, the size limitation imposed by the field of view of the microscope objective could be exceeded. Furthermore, the DOE's design, with a thickness of  $6.4~\mu m$ , enabled its fabrication within a

reasonable timeframe of 68.5 hours, which can be accomplished over the course of a weekend.

Thirdly, the measurements obtained from the beam profiler demonstrate the suitability of the calculated holograms for the purpose of beam shaping. This is evidenced by the successful generation two ring beams.

Fourthly, the conducted damage tests provide evidence that the 2PP structures are suitable for utilization at high average laser powers and pulse energies, which are necessary for micro material processing with ultrashort pulse laser systems. An average power of 22.8 W and a peak power intensity of 24.8 GW/cm² could be used without damaging the DOE.

These advances establish the prerequisites for future material processing experiments using 2PP fabricated DOEs.

The damage threshold may be increased further by reducing the yellow tint and consequently enhancing the transparency of the photoresist. This objective could be accomplished by incorporating an alternative photoinitiator within the photoresist or by completely removing the photoinitiator [34], although this approach may lead to a reduction in processing speed. Furthermore, the removal of the organic component of the utilized organic-inorganic hybrid photoresist through techniques such as calcination [35] might also result in the achievement of higher damage thresholds. Moreover, the beam shape could be enhanced through the utilization of objectives with a higher numerical aperture, thereby resulting in an improved surface quality. However, these objectives possess a smaller FOV, which would result in a substantial increase in fabrication time. Therefore, it is essential to establish a trade-off between processing time and the quality of the beam shape. Another option for increasing the surface quality would be to implement a post processing step like high temperature annealing [36], or coating by atomic layer deposition [37].

# **Acknowledgments and Appendixes**

The authors thank the German Federal Ministry of Education and Research (BMBF) (FKZ: 03VP09211, MINI2PP) and the German Federal Ministry for Economic Affairs and Energy (BMWE) (FKZ: 03EFNW0386) for financial support of this project.

#### References

- [1] G. Kontenis, D. Gailevičius, L. Jonušauskas, and V. Purlys: Opt. Express, 28, (2020) 27850.
- [2] A. Vyas, M. B. Roopashree, R. K. Banyal, and B. R Prasad: arXiv, 0909.3413 (2009).
- [3] C. Lutz, G. L. Roth, S. Rung, C. Esen, and R. Hellmann: J. Laser Micro Nanoeng, 16, (2021) 1.
- [4] M. Gafner, S. Remund, M. v. Chaja, T. Mähne, and B. Neuenschwander: Proc. CIRP, 94, (2020) 802.
- [5] Y. Yang, A. Forbes, and L. Cao: OES, 2, (2023) 230026.
- [6] S. N. Khonina, N. L. Kazanskiy, R. v. Skidanov, and M. A. Butt: Adv. Mater. Technol., 10, (2024) 2401028.
- [7] D. E. Aguiam, J. D. Santos, C. Silva, F. Gentile, C. Ferreira, I. S. Garcia, J. Cunha, and J. Gaspar: Micro Nano Eng., 14, (2022) 100111
- [8] A. Stemmer, H. Zarschizky, E. Knapek, G. Lefranc, and H. Scherer-Winner: Microelectron. Eng., 21, (1993) 471.

- [9] A. Jacobo-Martín, N. Jost, J. J. Hernández, C. Domínguez, G. Vallerotto, S. Askins, I. Antón, and I. Rodríguez: Opt. Express, 29, (2021) 34135.
- [10] M. T. Langridge, D. C. Cox, R. P. Webb, and V. Stolojan: Micron, 57, (2014) 56.
- [11] E. Tomono, H. Miyashita, T. Ono, and M. Esashi: Proc. Transducers 2009-International Solid-State Sensors, Actuators and Microsystems Conference, (2009) 853.
- [12] J. Li, P. Fejes, D. Lorenser, B. C. Quirk, P. B. Noble, R. W. Kirk, A. Orth, F. M. Wood, B. C. Gibson, D. D. Sampson, and R. A. McLaughlin: Sci. Rep., 8, (2018) 13789.
- [13] H. Wang, W. Zhang, D. Ladika, H. Yu, D. Gailevičius, H. Wang, C. F. Pan, P. N. S. Nair, Y. Ke, T. Mori, J. Y. E. Chan, Q. Ruan, M. Farsari, M. Malinauskas, S. Juodkazis, M. Gu, and J. K. W. Yang: Adv. Funct. Mater., 33, (2023) 2214211.
- [14] X. Zhou, Y. Hou, and J. Lin: AIP Adv., 5, (2015) 030701.
- [15] H. Wang, Y. Liu, Q. Ruan, H. Liu, R. J. H. Ng, Y. S. Tan, H. Wang, Y. Li, C. W. Qiu, and J. K. W. Yang: Adv. Opt. Mater., 7, (2019) 1900068.
- [16] P. Kiefer, V. Hahn, S. Kalt, Q. Sun, Y. M. Eggeler, and M. Wegener: Light Adv. Manuf., 4, (2024) 28.
- [17] J. Sandford O'Neill, P. Salter, Z. Zhao, B. Chen, H. Daginawalla, M. J. Booth, S. J. Elston, and S. M. Morris: Adv. Opt. Mater., 10, (2022) 2102446.
- [18] J. Marx, F. Behlau, D. Haske, C. Esen, and A. Ostendorf: Appl. Opt., 63, (2024), 6495.
- [19] H. D. Nguyen, E. Moreno, A. Rudenko, N. Faure, X. Sedao, C. Mauclair, J. P. Colombier, and R. Stoian: Sci. Rep., 12, (2022) 2074.
- [20] C. Lutz, S. Schwarz, J. Marx, C. Esen, and R. Hellmann: Photonics, 10, (2023) 413.
- [21] J. Fantova, A. Rodríguez, J. del Hoyo, G. G. Mandayo, and S. M. Olaizola: Opt. Laser Technol., 171, (2024) 110475.
- [22] N. Weber, D. Spether, A. Seifert, and H. Zappe: J. Opt. Soc. Am. A, 29, (2012) 808.
- [23] P. Ruchka, A. Kushwaha, J. A. Marathe, L. Xiang, R. Chen, R. Kirk, J. T. M. Tan, C. A. Bursill, J. Verjans, S. Thiele, R. Fitridge, R. A. McLaughlin, P. J. Psaltis, H. Giessen, J. Li: Adv. Photonics, 7, (2025) 026003
- [24] J. Liesener, M. Reicherter, T. Haist, and H. J. Tiziani: Opt. Commun., 185, (2000) 77.
- [25] R. Bowman, N. Muller, X. Zambrana-Puyalto, O. Jedrkiewicz, P. di Trapani, and M. J. Padgett: Eur. Phys. J. Spec. Top., 199, (2011) 159.
- [26] J. Marx, LAT Hologramm Software 2.3 (2024). https://doi.org/10.60517/t722h886m
- [27] A. D. Sinelnik, E. v. Bodyago, O. M. Kushchenko, I. I. Shishkin, N. K. Kuzmenko, D. S. Gets, and S. v. Makarov: Opt. Laser Technol., 171, (2024) 110411.
- [28] F. Behlau, J. Marx, C. Esen, and A. Ostendorf: Proc. LiM 2023 (2023). Manufacturing of a Fresnel axicon on a millimeter scale using two-photon polymerization.
- [29] G. Roy, and R. Tremblay: Opt. Commun., 34, (1980) 1.
- [30] I. Alexeev, K. H. Leitz, A. Otto, and M. Schmidt: Phys. Procedia, 5, (2010) 533.
- [31] M. Brown, and D. G. Lowe: Int. J. Comput. Vis., 74, (2007) 59.

- [32] K. Gourley, I. Golub, and B. Chebbi: Appl. Opt., 50, (2011) 303.
- [33] A. Butkutė, L. Čekanavičius, G. Rimšelis, D. Gailevičius, V. Mizeikis, A. Melninkaitis, T. Baldacchini, L. Jonušauskas, and M. Malinauskas: Opt. Lett., 45, (2020) 13.
- [34] D. Ladika, A. Butkus, V. Melissinaki, E. Skliutas, E. Kabouraki, S. Juodkazis, M. Farsari, and M. Malinauskas: Light Adv. Manuf., 5, (2024) 567.
- [35] D. Gailevicius, R. Zvirblis, K. Galvanauskas, G. Bataviciute, and M. Malinauskas: Photonics, 10, (2023) 597
- [36] N. Chidambaram, R. Kirchner, R. Fallica, L. Yu, M. Altana, and H. Schift: Adv. Mater. Technol., 2, (2017) 1700018.
- [37] D. Astrauskytė, K. Galvanauskas, D. Gailevičius, M. Drazdys, M. Malinauskas, and L. Grineviciute: Nanomaterials, 13, (2023) 2281.

(Received: June 27, 2025, Accepted: October 10, 2025)